

An in-frame deletion at the polymerase active site of *POLD1* causes a multisystem disorder with lipodystrophy

Michael N Weedon^{1,12}, Sian Ellard^{1,12}, Marc J Prindle^{2,12}, Richard Caswell¹, Hana Lango Allen¹, Richard Oram¹, Koumudi Godbole^{3,4}, Chittaranjan S Yajnik⁴, Paolo Sbraccia^{5,6}, Giuseppe Novelli^{5,6}, Peter Turnpenny⁷, Emma McCann⁸, Kim Jee Goh^{9,10}, Yukai Wang^{9,10}, Jonathan Fulford¹, Laura J McCulloch¹, David B Savage^{9,10}, Stephen O'Rahilly^{9,10}, Katarina Kos¹, Lawrence A Loeb^{2,11}, Robert K Semple^{9,10} & Andrew T Hattersley¹

DNA polymerase δ , whose catalytic subunit is encoded by *POLD1*, is responsible for lagging-strand DNA synthesis during DNA replication¹. It carries out this synthesis with high fidelity owing to its intrinsic 3'- to 5'-exonuclease activity, which confers proofreading ability. Missense mutations affecting the exonuclease domain of *POLD1* have recently been shown to predispose to colorectal and endometrial cancers². Here we report a recurring heterozygous single-codon deletion in *POLD1* affecting the polymerase active site that abolishes DNA polymerase activity but only mildly impairs 3'- to 5'-exonuclease activity. This mutation causes a distinct multisystem disorder that includes subcutaneous lipodystrophy, deafness, mandibular hypoplasia and hypogonadism in males. This discovery suggests that perturbing the function of the ubiquitously expressed *POLD1* polymerase has unexpectedly tissue-specific effects in humans and argues for an important role for *POLD1* function in adipose tissue homeostasis.

Progressive loss of subcutaneous adipose tissue, or lipodystrophy, with concomitant severe insulin resistance is a major feature of the recently described mandibular hypoplasia, deafness and progeroid features (MDP) syndrome³. Defining the genetic basis of this newly described form of progressive partial lipodystrophy would provide insights into the regulation of adipose tissue. Several genetic causes of partial lipodystrophy have previously been described⁴. Some of these affect genes with established roles in adipocyte differentiation or function, including *PPARG*, *PLIN1* and *CIDEA*. However, for other commonly implicated genes, including *LMNA* and *ZMPSTE24*, the link between the cellular defect and the adipose phenotype is poorly understood⁴. The mechanism underlying selective loss of only some adipose depots across all these conditions is also currently unclear.

Because all reported individuals with MDP syndrome have unrelated parents and no other affected family members, we hypothesized that the syndrome was caused by a heterozygous *de novo* mutation in a single gene. We therefore performed exome sequencing on two probands with MDP syndrome (Fig. 1 and Supplementary Table 1) and their unaffected parents to look for candidate *de novo* disease-causing mutations. Exonic sequences were enriched from genomic DNA using the Agilent SureSelect Human All Exon kit (version 4) and then sequenced on an Illumina HiSeq 2000 sequencer using 100-bp paired-end reads. We used Burrows-Wheeler aligner (BWA v0.6.2)⁵ to align sequence reads to the hg19 reference genome and the Genome Analysis Toolkit (GATK v2.2-10)⁶ to call single-nucleotide variants (SNVs) and indels. We covered 88% of targeted bases at >20 \times .

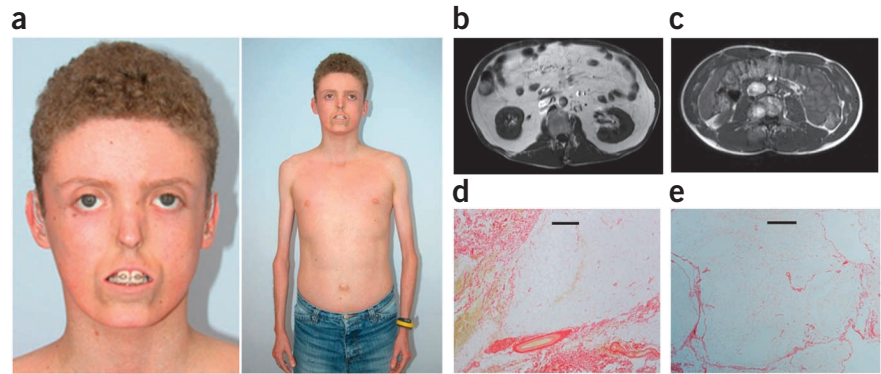
We identified an in-frame deletion (c.1812_1814delCTC, p.Ser605del) of a single codon in *POLD1* affecting the polymerase active site in both probands but in none of the four parents. We confirmed these results by Sanger sequencing (Online Methods). The c.1812_1814delCTC variant is absent from dbSNP137, the 1000 Genomes Project⁷ and the Exome Variant Server⁸. We then screened two additional individuals with MDP syndrome by Sanger sequencing and identified an identical in-frame deletion in both subjects. These findings provide convincing genetic evidence that the mutation encoding p.Ser605del is the disease-causing mutation in these four unrelated cases.

The most prominent phenotype of all four affected individuals was lack of subcutaneous adipose tissue, which was first noted in early childhood, although each proband was born with normal birth weight and appearance (Supplementary Table 1). The minimal subcutaneous adipose tissue at all sites contrasted with the marked increase in visceral adipose tissue (Fig. 1 and Supplementary Table 1). The ratio of visceral to subcutaneous adipose tissue was greatly elevated at 15.21 in subject 1 with MDP syndrome in contrast to the median

¹Institute of Biomedical and Clinical Science, University of Exeter Medical School, Exeter, UK. ²Joseph Gottstein Memorial Laboratory, Department of Pathology, University of Washington, Seattle, Washington, USA. ³Department of Genetic Medicine, Deenanath Mangeshkar Hospital and Research Center, Erandawane, Pune, India. ⁴Diabetes Unit, King Edward Memorial Hospital Research Center, Rasta Peth, Pune, India. ⁵Department of Biomedicine, Tor Vergata University, Rome, Italy. ⁶Department of Systems Medicine, Tor Vergata University, Rome, Italy. ⁷Clinical Genetics Department, Royal Devon and Exeter Hospital, Exeter, UK. ⁸Department of Clinical Genetics, Glan Clwyd Hospital, Rhyl, UK. ⁹Metabolic Research Laboratories, Institute of Metabolic Science, University of Cambridge, Cambridge, UK. ¹⁰National Institute for Health Research (NIHR) Cambridge Biomedical Research Centre, Institute of Metabolic Science, University of Cambridge, Cambridge, UK. ¹¹Department of Biochemistry, University of Washington, Seattle, Washington, USA. ¹²These authors contributed equally to this work. Correspondence should be addressed to A.T.H. (a.t.hattersley@exeter.ac.uk).

Received 27 March; accepted 22 May; published online 16 June 2013; doi:10.1038/ng.2670

Figure 1 Clinical characteristics of individuals with MDP syndrome. **(a)** Subject 1 (aged 15 years), demonstrating prominent lipodystrophy, small nose, 'pseudoproptosis' secondary to lack of subcutaneous periorbital fat, tight skin, mandibular hypoplasia, bilateral hearing aids and reduced limb muscles. Informed consent was obtained to publish this photograph. **(b,c)** Abnormal fat distribution in abdominal magnetic resonance imaging (MRI) at level L3 of subject 1 **(b)** and an age-, sex- and BMI-matched control **(c)** showing marked reduction of subcutaneous fat and increase in intra-abdominal fat in subject 1 as demonstrated by an increase in high-intensity signal. **(d,e)** Picosirius red staining of abdominal subcutaneous adipose tissue from subject 1 **(d)** and a representative comparative image of a BMI-matched subject **(e)**. Scale bars, 500 μm . Adipose tissue from subject 1 with a *POLD1* mutation shows a considerable amount of fibrosis (red staining). Full clinical details of all four affected individuals are presented in **Supplementary Table 1**.



value of 0.84 (interquartile range of 0.64–1.10) in 1,680 middle-aged men⁹. All affected individuals had clinical and biochemical evidence of insulin resistance, despite having body mass index (BMI) values of <20 kg/m². Other common clinical features included skin scleroderma and telangiectasia, ligament contractures, reduced mass of limb muscles, mandibular hypoplasia, hypogonadism and undescended testes in males, and sensorineural deafness (**Supplementary Table 1**). None of the affected individuals in our relatively young series or in a previous report³ has been diagnosed with cancer.

DNA polymerase δ has been shown to cooperate with WRN, a DNA helicase, to help maintain genome stability¹⁰. Loss of WRN function in humans leads to Werner syndrome, which presents with the premature onset of features associated with normal aging¹¹. Werner syndrome includes progressive loss of limb adipose tissue and fat with severe insulin resistance, prominent joint contractures, scleroderma, hypogonadism and pinched nose, similar to MDP syndrome. However, individuals with MDP syndrome lack several key features of Werner syndrome, including short stature, premature balding and/or graying and cataracts (**Supplementary Table 1** and ref. 11). Similarly, there are clear differences of MDP syndrome from the progeroid syndrome mandibular acral dysplasia (MAD), which is caused by mutations in *LMNA*¹² or *ZMPSTE24* (ref. 13), as individuals with MDP syndrome do not have short stature, premature hair loss, clavicle hypoplasia or acroosteolysis, and individuals with MAD do not have hearing loss.

DNA replication is fundamental to the successful division of all nucleated cells, and *POLD1*, which encodes the catalytic subunit of the key, processive lagging-strand polymerase, thus serves a ubiquitous and critical cellular function¹. Correspondingly, knockout of the mouse ortholog *Pold1* does not result in viable animals¹⁴. The tissue-specific effect of the heterozygous deletion mutation we have found is thus unexpected. *POLD1* mRNA was well expressed across a panel of human tissues, including muscle and fat, but differential expression did not account for the phenotype (**Supplementary Fig. 1**). Moreover, there was no evidence in the commonly used mouse 3T3-L1 model of adipogenesis that *Pold1* expression changed during the differentiation of preadipocytes into fat cells (**Supplementary Fig. 2**).

Subcutaneous abdominal adipose tissue from subject 1 (BMI of 19.1 kg/m²) showed abundant fibrosis dividing the remaining fat tissue but no obvious inflammatory cell infiltrates (**Fig. 1** and **Supplementary Fig. 3**). Consistent with this observation, the expression levels of key extracellular matrix genes were markedly different from those in five lean controls (BMI values of 20.0–21.8 kg/m²), with increased expression of transforming growth factor (TGF)- β (*TGFB1*), a hallmark of tissue fibrosis, and markedly higher expression of fibronectin (*FNI*) (**Supplementary Fig. 4**). Increased fibrosis has been correlated with adipose tissue dysfunction and insulin resistance in a variety of settings, including in individuals with lipodystrophy due to *PLIN1* mutations¹⁵ and common obesity¹⁶.

Figure 2 Protein schematic and modeling of *POLD1* alterations. **(a)** Schematic of the *POLD1* protein. Mutations predisposing to cancer (encoding p.Pro327Leu and p.Ser478Asn) affect residues within the exonuclease (proofreading) domain, whereas the mutation encoding p.Ser605del (found in four individuals with MDP syndrome) affects the polymerase active site. **(b)** Global structure of *POLD1* showing relevant alterations. The structure of *POLD1* (residues 77–983; modeled on template 3iay) is shown in ribbon form, colored by secondary structure succession (N terminus (blue) to C terminus (red)). The backbone and side chains are displayed in stick format for residues Pro327 and Ser478 (pink), Asp602 and Asp757 (yellow), Ser604 (dark green), Ser605 (red) and Leu606 (blue). The trinucleotide substrate is shown in stick format (light blue), with hydrogen bonds to the polymerase catalytic site indicated by green dashed lines. Template DNA has been omitted for clarity. **(c,d)** Detail of the polymerase catalytic site, shown from the same viewpoint as in **b**, for wild-type *POLD1* **(c)** and Ser605del mutant *POLD1* **(d)**. Note the predicted deformation of the catalytic domain and loss of hydrogen bonding to substrate in the Ser605del mutant compared to wild-type *POLD1*.

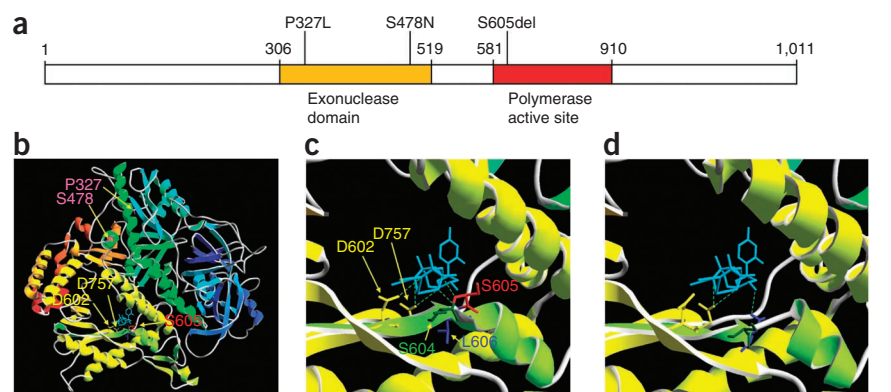
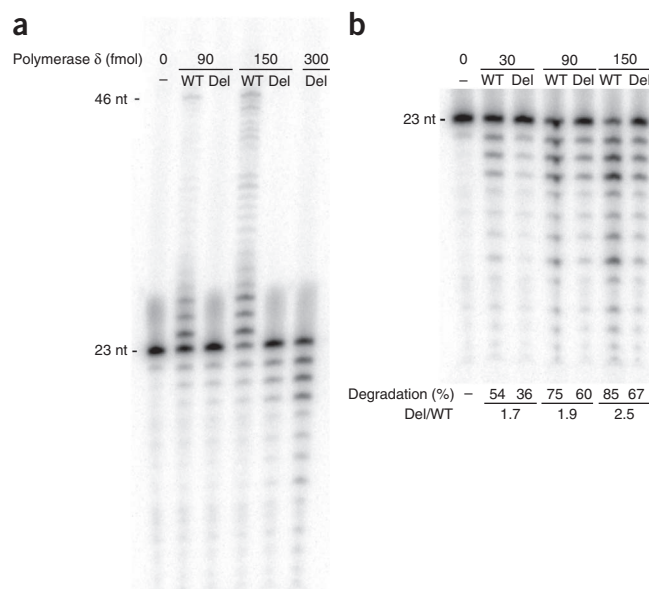


Figure 3 Polymerase δ with Ser605del mutant POLD1 has no detectable polymerase activity but has robust exonuclease activity. **(a)** Polymerase reactions using increasing concentrations of polymerase δ with either wild-type (WT) or Ser605del (del) POLD1 show that the mutant is incapable of extending the primer band (23 nt) in a 2-min reaction with 25 μ M of all four dNTPs. **(b)** Exonuclease reactions on the same 23-nt primer–46-nt template duplex DNA as in **a**, in the absence of dNTPs, show that polymerase δ with Ser605del mutant POLD1 exhibits a two- to threefold decrease in exonuclease activity compared to wild-type polymerase. Values for the percent of the primer band degraded reflect the results of three independent experiments and are derived from a comparison of the intensity of the primer band (P) and the exonuclease product bands (E), given by the following equation: percent degradation = $1 - (P/(P + E))$. The values of percent degradation for polymerase δ with Ser605del mutant POLD1 at 90, 150 and 300 fmol were plotted against the line obtained from measurements with the wild-type polymerase ($y = 0.0029x + 0.445$; $R^2 = 0.96$). The values derived indicate that ~1.7- to 2.5-fold more mutant enzyme is required to observe the same amount of primer degradation as with the wild-type enzyme under these experimental conditions.



The Ser605 deletion occurs in motif A, a highly conserved region of the polymerase δ catalytic subunit. This motif comprises 11 amino acids that are involved in the alignment of the incoming complementary dNTP with the primer terminus, as well as in the coordination and catalysis of phosphodiester bond formation¹⁷. Alterations in this domain have been shown to affect base selection and, consequently, polymerase fidelity in nearly every family of DNA polymerases from viruses to mammals^{18,19}. *In silico* modeling predicted that the Ser605 deletion profoundly affects the structure of the polymerase active site, in particular, by disrupting the hydrogen bonding between the substrate trinucleotide and the catalytic aspartate residues. As a comparison, the predicted structure of the catalytic site and bonding to the trinucleotide substrate were identical to those of wild-type POLD1 for both Pro327Leu and Ser478Asn mutants (data not shown). The proofreading domain was not predicted to be affected, in contrast to the expected changes previously reported for the cancer-predisposing mutations² (Fig. 2 and Online Methods). We therefore hypothesized that the Ser605del mutant polymerase would be able to bind DNA but not catalyze polymerization.

To test this hypothesis, we generated the Ser605 deletion mutant by PCR-mediated mutagenesis and purified the four-subunit human DNA polymerase δ holoenzyme from *Escherichia coli* (Online Methods). We quantified the polymerase activity of the purified enzyme by measuring primer elongation on a 23-nt primer–46-nt template duplex in the presence of all four dNTPs (Fig. 3a). Under conditions in which wild-type polymerase δ (150 fmol) extended 81% of the primer, DNA extension using the same amount of the mutant enzyme was not detected.

To assess the exonuclease activity of polymerase δ with wild-type and Ser605del mutant POLD1, we adapted the extension assay by excluding dNTPs. The exonuclease activity of the wild-type enzyme was linear in reactions using 30, 90 and 150 fmol of enzyme, and comparison of the amount of primer degradation using different amounts of mutant enzyme (90, 150 and 300 fmol) against this linear range showed that polymerase δ with Ser605del POLD1 had 1.7- to 2.5-fold lower exonuclease activity than wild-type polymerase (Fig. 3b). Despite this difference, the exonuclease activity of the mutant polymerase δ enzyme was considerable. Collectively, these findings demonstrate decoupling of the enzymatic activities of the mutant enzyme. Its preserved exonuclease activity indicates that it can bind DNA and suggests that the inability to extend DNA primers is due to an inability to efficiently interact with and incorporate dNTPs.

These results provide a possible molecular explanation for the markedly different phenotype caused by the Ser605 deletion compared to the previously described cancer predisposition mutations². Whereas the cancer-related mutations affect the proofreading domain and lead to increased base-substitution error rates², we show that polymerase δ with Ser605del POLD1 can bind to DNA but not catalyze polymerization. This is likely to result in an increase in stalled replication forks, which are associated with double-stranded DNA breaks, genomic instability, cell cycle checkpoint response and cell senescence and death²⁰. Preserved DNA binding by the mutant also raises the possibility that it may be able to compete with coexpressed wild-type polymerase, and previous work in yeast has shown that reduction in the amount of DNA polymerase δ leads to increased numbers of deletions and genomic instability^{21,22}. However, further work is required to understand how the mutation encoding the Ser605 deletion leads to the specific phenotype observed in the affected individuals with MDP syndrome.

There is some support for the notion of distinct phenotypes caused by mutations affecting different POLD1 domains from mouse models. Mice harboring a homozygous mutation in *Pold1* encoding p.Asp400Ala in the proofreading domain showed a tenfold increase in the base-substitution error rate over wild-type mice, and 94% of these mice developed cancer by the age of 18 months²³. In contrast, mice with a heterozygous substitution encoding p.Leu604Lys (equivalent to human p.Leu606Lys and neighboring the Ser605 residue deleted in individuals with MDP syndrome) showed an 18% reduction in lifespan, a small increase in tumorigenesis and a clear increase in chromosome aberrations¹⁹. Subsequent work suggested that this phenotype is due to an increase in the incidence of stalled replication forks, particularly at sites of DNA damage²⁴. Lipodystrophy was not reported in mice expressing the p.Leu604Lys mutant; however, it has proved very challenging to replicate other forms of partial lipodystrophy in mice, which may require extreme caloric loads to manifest metabolic disease²⁵.

In conclusion, whereas missense mutations of *POLD1* affecting the proofreading domain predispose to cancer, we show that a single-codon deletion in *POLD1* affecting the polymerase active site causes a markedly different phenotype that includes lipodystrophy. We further show that this mutation results in complete loss of polymerase activity but very little loss of exonuclease capacity. In addition to aiding in

understanding the basis of a complex syndrome, the Ser605del mutant POLD1 protein could serve as an important tool to explore more fundamental aspects of DNA polymerase biology.

URLs. SWISS-MODEL, <http://swissmodel.expasy.org/>; ImageJ64, <http://imagej.nih.gov/ij/>.

METHODS

Methods and any associated references are available in the [online version of the paper](#).

Accession codes. Human *POLD1* cDNA (NCBI), [NM_002691.3](#); yeast DNA polymerase δ crystal structure (Protein Data Bank), [3iay](#).

Note: Supplementary information is available in the online version of the paper.

ACKNOWLEDGMENTS

We thank M. Day, A. Damhuis and R. Gilbert for technical assistance. We thank K. Knapp for providing the data for the DEXA calculations. We thank L. Tung (University of Cambridge) for providing the human tissue whole-RNA panel. This work was supported by the NIHR Exeter Clinical Research Facility through funding for S.E. and A.T.H., and general infrastructure. S.E., A.T.H. and S.O. are supported by Wellcome Trust Senior Investigator awards 098395/Z/12/A and 098395/Z/12/Z. D.B.S. and R.K.S. are supported by Wellcome Trust Senior Research Fellowships in Clinical Science (098498/Z/12/Z). M.N.W. is supported by the Wellcome Trust as part of Wellcome Trust Biomedical Informatics Hub funding. R.O. is supported by Diabetes UK. D.B.S., R.K.S. and S.O. are supported by the UK NIHR Cambridge Biomedical Research Centre. K.J.G. is supported by the Agency for Science, Technology and Research, Singapore (A*STAR). Research reported in this publication by M.J.P. and L.A.L. was supported by the National Cancer Institute of the US National Institutes of Health under awards R01CA102029 and P01CA077852. The opinions in this paper are solely those of the authors and do not necessarily represent the views of the US National Institutes of Health, the Department of Health (England) or other funders.

AUTHOR CONTRIBUTIONS

S.E. and A.T.H. designed the study. M.N.W. and H.L.A. performed bioinformatics analyses. R.C. performed the exome sequencing and structural modeling. M.J.P., K.J.G., Y.W., J.E., L.J.M., L.A.L., K.K. and R.K.S. performed the functional studies. R.C. and S.E. performed the Sanger sequencing analysis and interpreted the results. R.O., K.G., C.S.Y., P.S., G.N., P.T., E.M., D.B.S., S.O., R.K.S. and A.T.H. analyzed the clinical data. M.N.W., S.E., M.J.P., R.K.S. and A.T.H. prepared the draft manuscript. All authors contributed to discussion of the results and manuscript preparation.

COMPETING FINANCIAL INTERESTS

The authors declare no competing financial interests.

Reprints and permissions information is available online at <http://www.nature.com/reprints/index.html>.

1. Prindle, M.J. & Loeb, L.A. DNA polymerase delta in DNA replication and genome maintenance. *Environ. Mol. Mutagen.* **53**, 666–682 (2012).

2. Palles, C. *et al.* Germline mutations affecting the proofreading domains of POLE and POLD1 predispose to colorectal adenomas and carcinomas. *Nat. Genet.* **45**, 136–144 (2013).
3. Shastry, S. *et al.* A novel syndrome of mandibular hypoplasia, deafness, and progeroid features associated with lipodystrophy, undescended testes, and male hypogonadism. *J. Clin. Endocrinol. Metab.* **95**, E192–E197 (2010).
4. Semple, R.K., Savage, D.B., Cochran, E.K., Gorden, P. & O'Rahilly, S. Genetic syndromes of severe insulin resistance. *Endocr. Rev.* **32**, 498–514 (2011).
5. Li, H. & Durbin, R. Fast and accurate short read alignment with Burrows-Wheeler transform. *Bioinformatics* **25**, 1754–1760 (2009).
6. McKenna, A. *et al.* The Genome Analysis Toolkit: a MapReduce framework for analyzing next-generation DNA sequencing data. *Genome Res.* **20**, 1297–1303 (2010).
7. Abecasis, G.R. *et al.* An integrated map of genetic variation from 1,092 human genomes. *Nature* **491**, 56–65 (2012).
8. Fu, W. *et al.* Analysis of 6,515 exomes reveals the recent origin of most human protein-coding variants. *Nature* **493**, 216–220 (2013).
9. Kaess, B.M. *et al.* The ratio of visceral to subcutaneous fat, a metric of body fat distribution, is a unique correlate of cardiometabolic risk. *Diabetologia* **55**, 2622–2630 (2012).
10. Kamath-Loeb, A.S., Shen, J.C., Schmitt, M.W. & Loeb, L.A. The Werner syndrome exonuclease facilitates DNA degradation and high fidelity DNA polymerization by human DNA polymerase δ . *J. Biol. Chem.* **287**, 12480–12490 (2012).
11. Oshima, J., Martin, G.M. & Hisama, F.M. Werner syndrome. *GeneReviews* <<http://www.ncbi.nlm.nih.gov/books/NBK1514/>> (2012).
12. Novelli, G. *et al.* Mandibuloacral dysplasia is caused by a mutation in *LMNA*-encoding lamin A/C. *Am. J. Hum. Genet.* **71**, 426–431 (2002).
13. Agarwal, A.K., Fryns, J.P., Auchus, R.J. & Garg, A. Zinc metalloproteinase, *ZMPSTE24*, is mutated in mandibuloacral dysplasia. *Hum. Mol. Genet.* **12**, 1995–2001 (2003).
14. Uchimura, A., Hidaka, Y., Hirabayashi, T., Hirabayashi, M. & Yagi, T. DNA polymerase delta is required for early mammalian embryogenesis. *PLoS ONE* **4**, e4184 (2009).
15. Gandotra, S. *et al.* Perilipin deficiency and autosomal dominant partial lipodystrophy. *N. Engl. J. Med.* **364**, 740–748 (2011).
16. Henegar, C. *et al.* Adipose tissue transcriptomic signature highlights the pathological relevance of extracellular matrix in human obesity. *Genome Biol.* **9**, R14 (2008).
17. Swan, M.K., Johnson, R.E., Prakash, L., Prakash, S. & Aggarwal, A.K. Structural basis of high-fidelity DNA synthesis by yeast DNA polymerase δ . *Nat. Struct. Mol. Biol.* **16**, 979–986 (2009).
18. Reha-Krantz, L.J. & Nonay, R.L. Motif A of bacteriophage T4 DNA polymerase: role in primer extension and DNA replication fidelity. Isolation of new antimutator and mutator DNA polymerases. *J. Biol. Chem.* **269**, 5635–5643 (1994).
19. Venkatesan, R.N. *et al.* Mutation at the polymerase active site of mouse DNA polymerase δ increases genomic instability and accelerates tumorigenesis. *Mol. Cell. Biol.* **27**, 7669–7682 (2007).
20. Branzei, D. & Foiani, M. Maintaining genome stability at the replication fork. *Nat. Rev. Mol. Cell Biol.* **11**, 208–219 (2010).
21. Kokoska, R.J., Stefanovic, L., DeMai, J. & Petes, T.D. Increased rates of genomic deletions generated by mutations in the yeast gene encoding DNA polymerase δ or by decreases in the cellular levels of DNA polymerase δ . *Mol. Cell. Biol.* **20**, 7490–7504 (2000).
22. Lemoine, F.J., Degtyareva, N.P., Kokoska, R.J. & Petes, T.D. Reduced levels of DNA polymerase δ induce chromosome fragile site instability in yeast. *Mol. Cell. Biol.* **28**, 5359–5368 (2008).
23. Goldsby, R.E. *et al.* High incidence of epithelial cancers in mice deficient for DNA polymerase δ proofreading. *Proc. Natl. Acad. Sci. USA* **99**, 15560–15565 (2002).
24. Schmitt, M.W. *et al.* Active site mutations in mammalian DNA polymerase δ alter accuracy and replication fork progression. *J. Biol. Chem.* **285**, 32264–32272 (2010).
25. Savage, D.B. Mouse models of inherited lipodystrophy. *Dis. Model. Mech.* **2**, 554–562 (2009).

ONLINE METHODS

Subjects. Individuals with MDP syndrome were identified by their clinicians and referred for molecular genetic analysis in the Exeter Molecular Genetics Laboratory. All subjects gave informed consent for genetic testing, and the study was approved by the North Wales Research Ethics Committee.

Exome sequencing. Exonic sequences were enriched from genomic DNA using Agilent's SureSelect Human All Exon kit (version 4) and then sequenced on an Illumina HiSeq 2000 sequencer using 100-bp paired-end reads. We used BWA (v0.6.2)⁵ to align sequence reads to the hg19 reference genome and GATK (v2.2-10)⁶ to call SNVs and indels.

Sanger sequencing confirmation. We amplified *POLD1* exon 15 using the primers whose sequences are listed in **Supplementary Table 2**. PCR products were sequenced on an ABI3730 capillary machine (Applied Biosystems) and analyzed using Mutation Surveyor v3.98 (SoftGenetics).

Protein modeling. The sequence of full-length *POLD1* was submitted for automated modeling and template selection using the SWISS-MODEL web interface. This returned a structure for *POLD1* residues 77–983 based on template 3iay, chain A (*Saccharomyces cerevisiae* DNA polymerase δ , catalytic subunit; 49% sequence identity), which was the same template used for the model of human *POLD1* in the Protein Model Portal database (P28340). Subsequently, all modeling of mutant sequences was carried out using template 3iay (chain A), and structures were visualized in the Swiss-PdbViewer.

Human tissue expression profiling. A human tissue whole-RNA panel was purchased from AMS Biotechnology and was provided by L. Tung. cDNA synthesis was performed using the ImProm-IITM Reverse Transcription System (Promega) according to the manufacturer's recommendation. Human *POLD1* mRNA and 18S rRNA levels were determined using TaqMan Gene Expression assays (Hs01100821_m1 for *POLD1* and custom designed for 18S (sequences available upon request); Applied Biosystems). Serially diluted human cDNA was used to generate a standard curve for each assay, and all RNA determinations were performed in duplicate using TaqMan PCR Master Mix on an ABI 7900 detection system (Applied Biosystems). *POLD1* mRNA expression levels were normalized to the levels of 18S rRNA for comparison between tissues.

3T3-L1 differentiation time course. 3T3-L1 cells (American Type Culture Collection) were cultured in DMEM supplemented with 10% NCS, 100 U/l penicillin, 100 μ g/ml streptomycin, 4 mM L-glutamine and 4 mg/ml puromycin (Sigma) in a humidified incubator with 5% CO₂ at 37 °C. Preadipocyte differentiation was induced by growing cells for 2 d after they reached confluence and exposing them to medium in which FBS replaced NCS that was supplemented for the first 3 d with 500 μ M IBMX, 1 μ M dexamethasone (Sigma-Aldrich) and 100 nM soluble human insulin (Novo Nordisk) and for the next 3 d with 100 nM insulin only, with no supplements thereafter. Total RNA was extracted using an RNeasy mini kit (Qiagen) at the time points indicated. mRNA levels of *Pold1* were determined using an inventoried TaqMan Gene Expression assay (Hs01100821_m1; Applied Biosystems), and levels of *Adipoq* and cyclophilin A were determined using custom-designed TaqMan Gene Expression assays (sequences available upon request). Quantitative RT-PCR assays were undertaken as described, and mRNA levels for the genes of interest were normalized to those of cyclophilin A (*PPIA*) for comparison. Three time courses were undertaken in duplicate. Results shown are the mean levels with s.e.m. from these biological replicates.

Expression and fibrosis studies from fat. Abdominal subcutaneous adipose tissue biopsies were obtained from subject 1 (BMI of 19.1 kg/m²) from below and lateral to the umbilicus and from five healthy, lean controls of European ancestry (BMI range of 20.0–21.8 kg/m²) obtained during elective surgery and with consent and ethical approval from the NIHR Exeter Tissue Bank. Biopsies were immediately snap frozen in liquid nitrogen and stored at –80 °C until processing. Total RNA was extracted using the phenol-chloroform-guanidinium-thiocyanate method²⁶. Briefly, ~100 mg of tissue was homogenized in TRI reagent (Life Technologies) using a Retsch Mixer Mill MM400 in accordance with the manufacturer's instructions, and RNA concentrations were determined spectrophotometrically using Nanodrop technology. RNA was

treated with DNase to remove residual genomic contamination, and 500 ng was reverse transcribed in a random-primed single-strand synthesis reaction using high-capacity reverse transcriptase (Life Technologies).

cDNA was diluted 1:20 in 0.01 M Tris-HCl, and amplification was performed using Universal PCR Master Mix (Life Technologies) and extracellular matrix gene-specific probes (probe sequences available upon request). All samples were amplified in triplicate for each assay and were run alongside a standard curve to allow assay efficiency determination. Samples amplified in the absence of reverse transcriptase enzyme and samples without template were used as negative controls. Amplification was performed using an ABI 7900 thermal cycler with the following cycling parameters: 50 °C for 2 min, 95 °C for 10 min and 40 cycles of 95 °C for 15 s and 60 °C for 1 min. Gene expression levels were calculated using the 2^{– $\Delta\Delta$ CT} analysis method modified by Pfaffl²⁷, normalizing to the levels of the adipose-specific housekeeping genes *PPIA* and *UBC*²⁸.

For fibrosis studies, fat tissue biopsies from subject 1, as well as from a lean individual (BMI of 20 kg/m²) and an obese individual (BMI of 43.6 kg/m²) obtained during elective surgery, were formalin fixed, paraffin embedded and stained with picrosirius red (Sigma-Aldrich) for fibrosis as previously described¹⁶.

MRI. Abdominal images were collected via an MRI T1 (spin-lattice relaxation time)-weighted breath-hold sequence to obtain images with high fat contrast. Subcutaneous and visceral fat volumes were calculated via semi-automated processing based on signal intensity thresholding between the L5/S1 disk and the bottom of the lung.

Site-directed mutagenesis. The 3-nucleotide deletion was introduced into the pET303-hpold1 plasmid²⁹ using 5'-phosphorylated primers flanking the deletion site (**Supplementary Table 3**). PCR products were gel purified and ligated before transformation into XL10-Gold Ultracompetent Cells (Stratagene). A region between the AgeI and ClaI sites of *POLD1* was amplified and sequence verified, and this region was then subcloned back into AgeI- and ClaI-digested pET303-hpold1 vector that had not been PCR amplified.

Purification of polymerase δ with Ser605del *POLD1*. The mutant polymerase δ holoenzyme was purified as described³⁰. Briefly, the pET303-hpold1 plasmid and the pCOLA-2, pCOLA-3 and pCOLA-4 plasmids, with sequences encoding the p66, p55 and p12 subunits of the polymerase δ holoenzyme, respectively, were cotransformed into BL21-tRARE cells by electroporation. Protein expression was induced in mid-log phase cells by the addition of β -D-1-thiogalactopyranoside (IPTG). Cells were sonicated, and the crude extract was subjected to nickel column (Novagen) chromatography in which polymerase δ was bound via the polyhistidine tag on the p12 subunit. Bound enzyme was eluted with 300 mM imidazole and was further purified by ion exchange chromatography on a HiTrap SP HP column (GE) using a linear (0.2–1.0 M) NaCl gradient.

Polymerase and exonuclease assays. The polymerase and exonuclease activities of wild-type polymerase δ and polymerase δ with Ser605del mutant *POLD1* were measured using the same reaction mixtures and enzyme dilutions. Reactions included the indicated concentrations of enzyme, 40 mM Tris-HCl (pH 7.4), 4 mM MgCl₂, 0.1 mg/ml BSA, 5 mM DTT, 25 μ M each dNTP (polymerase reactions only) and 10 nM 5' end-labeled primer-template DNA duplex (**Supplementary Table 4**). Reactions were incubated for 2 min at 37 °C and stopped by the addition of 95% formamide in 20 mM EDTA. Samples were resolved on a 14% polyacrylamide TBE-urea gel; reaction products were visualized following imaging on a PhosphorImager (Molecular Dynamics) and analyzed using ImageJ64 software.

- Chomczynski, P. & Sacchi, N. Single-step method of RNA isolation by acid guanidinium thiocyanate-phenol-chloroform extraction. *Anal. Biochem.* **162**, 156–159 (1987).
- Pfaffl, M.W. A new mathematical model for relative quantification in real-time RT-PCR. *Nucleic Acids Res.* **29**, e45 (2001).
- Neville, M.J., Collins, J.M., Gloy, A.L., McCarthy, M.I. & Karpe, F. Comprehensive human adipose tissue mRNA and microRNA endogenous control selection for quantitative real-time-PCR normalization. *Obesity (Silver Spring)* **19**, 888–892 (2011).
- Fazlieva, R. *et al.* Proofreading exonuclease activity of human DNA polymerase δ and its effects on lesion-bypass DNA synthesis. *Nucleic Acids Res.* **37**, 2854–2866 (2009).
- Schmitt, M.W., Matsumoto, Y. & Loeb, L.A. High fidelity and lesion bypass capability of human DNA polymerase δ . *Biochimie* **91**, 1163–1172 (2009).